

Increasing contribution of evaporative demand to future intensified drought across global drylands

Xiaojing Yu¹, Lixia Zhang², Tianjun Zhou³, Dan Zhao¹, and Ziming Chen¹

¹LASG, Institute of Atmospheric Physics, Chinese Academy of Sciences

²LASG, Institute of Atmospheric Physics Chinese Academy of Sciences

³IAP

November 22, 2022

Abstract

Drylands face more threat from droughts under global warming. It remains insufficient in quantifying the roles of potential evapotranspiration (PET) and precipitation (P) to drought changes in a warming climate. Thus, we quantified the relative contributions of PET and P and projected their future changes across global drylands under four scenarios from Phase Six of the Coupled Model Intercomparison Project (CMIP6) models. In the 21st century, the multimodel medians of hydroclimatic fields indicate relatively consistent trend patterns, showing a drying over most of global drylands except for East Asia, Middle East, Sahel and South Asia drylands. The standardized precipitation evapotranspiration index (SPEI) presents a robust and ubiquitous drying with scenario-dependent magnitudes. The fractional contributions of PET and P to the present-day drought changes are estimated to be approximately equal (~50%). For the near- and mid-term projections, PET (P) contributes ~58% (42%) and ~61% (~39%), respectively. In the long-term, the fractional contribution of PET (P) reaches ~65% (~35%), ~72% (28%), ~80% (~20%), ~85% (~15%) under four different scenarios, respectively. Furthermore, PET contributes more significantly in the North Hemisphere than in the South Hemisphere, particularly over the Mediterranean, central and East Asian drylands. Drought conditions tend to be relatively stable under low scenarios (SSP1-2.6 and SSP2-4.5), while exacerbate continuously under high scenarios (SSP3-7.0 and SSP5-8.5). By the end of 21st century, severe droughts like the present-day 1-in-20-yr events are estimated to become fairly common across global drylands. These results provide further understanding for making policy and adaption strategies for drylands.

1
2
3
4
5
6
7
8
9
10
11
12
13
14
15
16
17
18
19

**Increasing contribution of evaporative demand to future
intensified drought across global drylands**

Xiaojing Yu^{1,2}, Lixia Zhang¹, Tianjun Zhou^{1,2,3}, Dan Zhao^{1,2},
Ziming Chen^{1,2}

¹LASG, Institute of Atmospheric Physics, Chinese Academy of Sciences, Beijing,
China

²University of the Chinese Academy of Sciences, Beijing, China

To be submitted to Earth's Future

* Corresponding author: lixiazhang@mail.iap.ac.cn

20 **ABSTRACT**

21 Drylands face more threat from droughts under global warming. It remains
22 insufficient in quantifying the roles of potential evapotranspiration (PET) and
23 precipitation (P) to drought changes in a warming climate. Thus, we quantified the
24 relative contributions of PET and P and projected their future changes across global
25 drylands under four scenarios from Phase Six of the Coupled Model Intercomparison
26 Project (CMIP6) models. In the 21st century, the multimodel medians of hydroclimatic
27 fields indicate relatively consistent trend patterns, showing a drying over most of
28 global drylands except for East Asia, Middle East, Sahel and South Asia drylands. The
29 standardized precipitation evapotranspiration index (SPEI) presents a robust and
30 ubiquitous drying with scenario-dependent magnitudes. The fractional contributions
31 of PET and P to the present-day drought changes are estimated to be approximately
32 equal (~50%). For the near- and mid-term projections, PET (P) contributes ~58%
33 (42%) and ~61% (~39%), respectively. In the long-term, the fractional contribution of
34 PET (P) reaches ~65% (~35%), ~72% (28%), ~80% (~20%), ~85% (~15%) under
35 four different scenarios, respectively. Furthermore, PET contributes more significantly
36 in the North Hemisphere than in the South Hemisphere, particularly over the
37 Mediterranean, central and East Asian drylands. Drought conditions tend to be
38 relatively stable under low scenarios (SSP1-2.6 and SSP2-4.5), while exacerbate
39 continuously under high scenarios (SSP3-7.0 and SSP5-8.5). By the end of 21st
40 century, severe droughts like the present-day 1-in-20-yr events are estimated to
41 become fairly common across global drylands. These results provide further
42 understanding for making policy and adaption strategies for drylands.

43

44

45

46

47

48

49 **Plain Language Summary**

50 Drought is an essential natural hazard and even more damaging over the
51 drought-prone drylands. The hydroclimatic fields present regional discrepancies in the
52 sign of future trend, drying over North America, South America, Mediterranean,
53 central Asia, Southern Africa and Australia drylands, while wetting over East Asia,
54 Middle East, Sahel, and South Asia drylands. Additionally, the standardized
55 precipitation evapotranspiration index (SPEI), comprising the impacts of precipitation
56 and potential evapotranspiration, shows a robust and ubiquitous drying across global
57 drylands. Under different warming levels, the future contributions of the potential
58 evapotranspiration (PET) and precipitation tend to increase and decline with time,
59 respectively. In general, PET contributes more significantly over drylands in the North
60 Hemisphere than in the South Hemisphere, in regards to their nearly equal roles in the
61 20th century. Basically, projections by CMIP6 models indicate more widespread,
62 intense and frequent droughts across global drylands, which is mainly attributed to the
63 substantially increased PET in a warming climate.

64

65

66 **Key points:**

- 67 ● Hydroclimatic fields present a drying over most of global drylands except for
68 East Asia, Middle East, Sahel and South Asia drylands.
- 69 ● Fractional contribution of PET (precipitation) across global drylands is expected
70 to increase (decrease) with time under different scenarios.
- 71 ● Severe droughts like the present-day 1-in-20-yr events are estimated to become
72 fairly common across global drylands by the end of 21st century.

73

74 **1 Introduction**

75 Drought is a slow-onset but damaging hydroclimatic hazard with broad
76 spatio-temporal scales (Gill & Malamud, 2014; Ault, 2020). Severe droughts have
77 cascading impacts not only on environmental systems (Vicente-Serrano et al., 2020),
78 but also on socioeconomic development (Liu & Chen, 2021). Drylands,
79 drought-prone regions characterized by scarce precipitation (P) and high evaporative
80 demand [measured by potential evapotranspiration (PET)], occupy ~41% of global
81 terrestrial land (White & Nackoney, 2003) and are home to ~38% of the world's total
82 population [United Nations Development Programme (UNDP), 2014]. For their
83 vulnerable ecosystems and low societal resilience, drylands face more threat than
84 humid regions once hit by droughts, such as water and food deficits, population
85 migrations and international disputes (Mannava et al., 2013; Barlow et al., 2016; Ault,
86 2020; Fragaszy et al., 2020). Therefore, knowledge of the risks and severity for future
87 droughts is a prerequisite to make policies and adaption strategies in drylands.

88

89 Global widespread aridity has increased substantially since the 1980s in terms of
90 both hydrological fields (i.e., P, runoff, and soil moisture) and drought indices,
91 although with somewhat regional inhomogeneity (Dai, 2013, 2021; Trenberth et al.,
92 2014; Dai & Zhao, 2017). The key factor exacerbating land drying is attributed to the
93 land-atmosphere feedbacks in response to greenhouse warming (Sherwood & Fu,
94 2014; Berg et al., 2016). Legions of recent studies have projected robust increase in
95 intensity, frequency, and duration of droughts in a warmer climate (Lehner et al., 2017;
96 Zhou et al., 2019; Hari et al., 2020; Takeshima et al., 2020; Ukkola et al., 2020),
97 which is dominated by the warming-induced PET (Cook et al., 2014; Fu & Feng,
98 2014; Scheff & Frierson, 2015; Milly & Dunne, 2016; Zhao & Dai, 2017; Dai et al.,
99 2018; Spinoni et al., 2020). Some researchers have assessed the relative contributions
100 of P and PET to the magnitude and extent of global terrestrial aridity (Cook et al.,

101 2014; Scheff & Frierson, 2015). However, little has been done to reveal how their
102 contributions will change in a warming climate, especially in those regions where
103 changes in P and PET offset each other.

104

105 Under climate change, drylands experienced a more evident warming in the last
106 century, accounting for more than half of the continental warming (Huang et al., 2012;
107 Ji et al., 2014). For the intensified land-atmosphere feedbacks, drylands response
108 more dramatically to climate change (Huang et al., 2017a, 2017b; Wei et al., 2019),
109 such as accelerated expansion (Feng & Fu, 2013; Huang et al., 2015), higher risks of
110 degradation and desertification (Yao et al., 2020; Huang et al., 2020; Burrell et al.,
111 2020). Relatively few studies have addressed the future drought changes across global
112 drylands (Schlaepfer et al., 2017; Miao et al., 2020). Therefore, we focus on the two
113 questions in this study: (1) To what extent, P and PET contribute to future drought
114 changes throughout the global drylands? (2) How severe will droughts impact
115 drylands in a warming climate?

116

117 In the following, Section 2 describes the data and methods used in this study.
118 Subsequently, detailed results are illustrated in Section 3. To the end, we summarize
119 and discuss the results in Section 4.

120 **2 Data and methods**

121 **2.1 Observation and definition of drylands**

122 We use the Climatic Research Unit gridded Time Series Version 4.03 (CRU TS
123 v.4.03) with a spacial resolution of 0.5° latitude \times 0.5° longitude (Harris et al., 2020),
124 which is available at http://data.ceda.ac.uk/badc/cru/data/cru_ts/cru_ts_4.03. Two
125 variables including the observed P and derived PET during 1960–2018 are applied to
126 define the global drylands.

127

128 Drylands are generally defined by the aridity index (AI), which is the ratio of
129 annual P to PET (Middleton & Thomas, 1992; Hulme, 1996; Feng & Fu, 2013; Huang
130 et al., 2015). Here global drylands are measured as regions with AI less than 0.65 for
131 the 1960–2018 climatology, in line with the previous studies (Feng & Fu, 2013;
132 Huang et al., 2015).

133 **2.2 Standardized precipitation evapotranspiration index (SPEI)**

134 In this study, drought is quantified by the standardized precipitation
135 evapotranspiration index (SPEI, Vicente-Serrano et al., 2010). This index considers
136 both P and evaporative demand, and can be calculated on different time scales to
137 characterize different types of droughts (Vicente-Serrano et al., 2012). Here the
138 12-month SPEI is applied to measure the long-lasting drought for its detrimental
139 impacts on society and ecology. Droughts are then divided into mild ($-0.5 \leq \text{SPEI} < -1.0$),
140 moderate ($-1.0 \leq \text{SPEI} < -1.5$), severe ($-1.5 \leq \text{SPEI} < -2.0$) and extreme ($\text{SPEI} \leq -2.0$)
141 droughts (Vicente-Serrano et al., 2010). Among numerous ways to estimate PET (Xie
142 & Wang, 2020), we use the Penman–Monteith method, based on surface moisture and
143 energy balance considerations, recommended by the Food and Agricultural
144 Organization (FAO) of the United Nations (Penman 1948; Monteith 1965; Zotarelli et
145 al., 2013).

146 **2.3 CMIP6 models**

147 We use model outputs from the Coupled Model Intercomparison Project Phase 6
148 (CMIP6, <https://esgf-node.llnl.gov/search/cmip6/>), including historical simulations
149 and projections under four combined scenarios of the Shared Socioeconomic
150 Pathways (SSP) and the Representative Concentration Pathways (RCP), i.e., SSP1-2.6,
151 SSP2-4.5, SSP3-7.0, SSP5-8.5 scenarios (Eyring et al., 2016; O’Neil et al., 2016,
152 2017). Given the data availability for calculating PET, monthly variables from one
153 realization of 13 CMIP6 models are selected (Table.1). All outputs are regridded to
154 1.5° latitude \times 1.5° longitude via bilinear interpolation. Variables including P,

155 evapotranspiration (E), surface soil moisture content (SM) are applied to analyze the
 156 future changes for hydroclimate. SM is unavailable from INM-CM4-8 and
 157 INM-CM5-0. Variables, including near surface air temperature, specific humidity,
 158 wind, radiation, are applied to estimate PET. Moreover, four specific periods are
 159 examined and termed as the present day (1995–2014), near-term (2021–2040),
 160 mid-term (2041–2060), and long-term (2051–2100), respectively.

161

162

Table 1 Details of CMIP6 models used in this study

No	Model	Institute (Country)	Lat × Lon
1	ACCESS-CM2	Commonwealth Scientific and Industrial Research Organization and Bureau of Meteorology (Australia)	144×192
2	ACCESS-ESM1-5		145×192
3	BCC-CSM2-MR	Beijing Climate Center (China)	160×320
4	CanESM5	Canadian Centre for Climate Modelling and Analysis (Canada)	64×128
5	FGOALS-f3-L	Institute of Atmospheric Physics, Chinese Academy of Sciences (China)	180 x 360
6	INM-CM4-8	Institute for Numerical Mathematics, Russia	120 x 180
7	INM-CM5-0		
8	IPSL-CM6A-LR	Institute Pierre Simon Laplace (France)	143 x 144
9	MIROC6	Atmosphere and Ocean Research Institute (The University of Tokyo), National Institute for Environmental Studies, and Japan Agency for Marine-Earth Science and Technology (Japan)	128 x 256
10	MIROC-ES2L		64 x 128
11	MPI-ESM1-2-HR	Max Planck Institute for Meteorology (MPI-M)	192 x 384
12	MPI-ESM1-2-LR		96 x 192
13	MRI-ESM2-0	Meteorological Research Institute (Japan)	96 x 192

163 2.4 Analysis methods

164 In the process of calculating SPEI, the baseline period is set to 1960–1989 because the
 165 observed drought area and frequency increase remarkably since the 1990s across

166 global drylands (Vicente-Serrano et al., 2010; Dai, 2011; Dai & Zhao, 2017). To
167 quantify the relative contributions of PET and P, we calculate four versions of SPEI
168 for 1900–2100 following as Cook et al. (2014). They are termed as SPEI_All,
169 SPEI_PET, SPEI_P and SPEI_Sum, respectively. First, we calculate SPEI using P and
170 estimated PET from model outputs, which incorporates changes in both P and PET,
171 referred as SPEI_All. Secondly, we isolate the impact of PET (P) by detrending
172 monthly P (PET) during 1990–2100 and setting the mean to be equal to the
173 1960–1989 climatology. Then, SPEI_PET (SPEI_P), only considering the impact of
174 PET (P), is calculated by using PET (P) and the detrended P (PET). Finally,
175 SPEI_Sum, the sum of SPEI_PET and SPEI_P, is calculated to compare with
176 SPEI_All. SPEI_Sum is higher than SPEI_All because P and PET are not completely
177 independent, in accord with Cook et al. (2014). Overall, SPEI_Sum and SPEI_All are
178 consistent enough to be used to investigate the respective impact of PET and P.

179

180 The relative contributions of P and PET to SPEI are ultimately expressed as the
181 following formula:

$$182 \quad \text{SPEI_Sum} = \text{SPEI_PET} + \text{SPEI_P} \quad (1)$$

$$183 \quad \Delta\text{SPEI_Sum} = \Delta\text{SPEI_PET} + \Delta\text{SPEI_P} \quad (2)$$

$$184 \quad \text{Perc(PET)} = \Delta\text{SPEI_PET} / \Delta\text{SPEI_Sum} \quad (3)$$

$$185 \quad \text{Perc(P)} = \Delta\text{SPEI_P} / \Delta\text{SPEI_Sum} \quad (4)$$

186 where Δ indicates SPEI changes relative to the 1960–1989 baseline. Perc(PET) and
187 Perc(P) are the contribution of changes in PET and P to changes in SPEI, respectively.

188

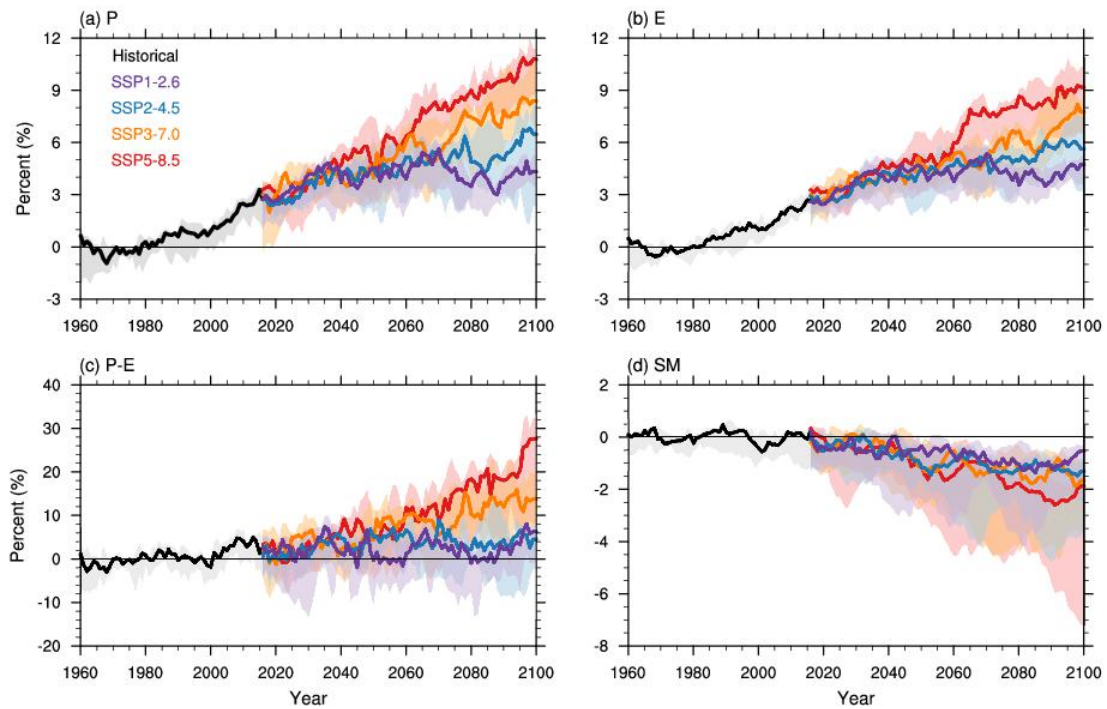
189 **3 Results**

190 **3.1 Future changes in hydroclimate**

191 We first analyze the projected changes of hydroclimatic fields area-averaged over

192 global drylands (Figure 1). Besides P and E, we also examine the future changes of
 193 surface water availability, namely precipitation minus evapotranspiration (P-E), and
 194 surface soil moisture (SM) for their indication in agricultural and hydrological
 195 droughts (Zhao & Dai, 2015; Cook et al., 2020; Zhou et al., 2021). P, E and P-E tend
 196 to increase consistently, more robust under the two high scenarios than the two low
 197 scenarios. Nevertheless, SM presents a relatively slight decreasing with much larger
 198 model uncertainties. By the end of the 21st century, the multi-model median projects
 199 an increase of ~4, 5, 8 and 10% for P, ~4, 5, 6 and 9 % for E, ~2, 4, 10, and 20% for
 200 P-E, whereas a decline of ~1, 1, 1.5 and 2% for SM under SSP1-2.6, SSP2-4.5,
 201 SSP3-7.0 and SSP5-8.5 scenarios, respectively, relative to the 1960–1989
 202 climatology.

203



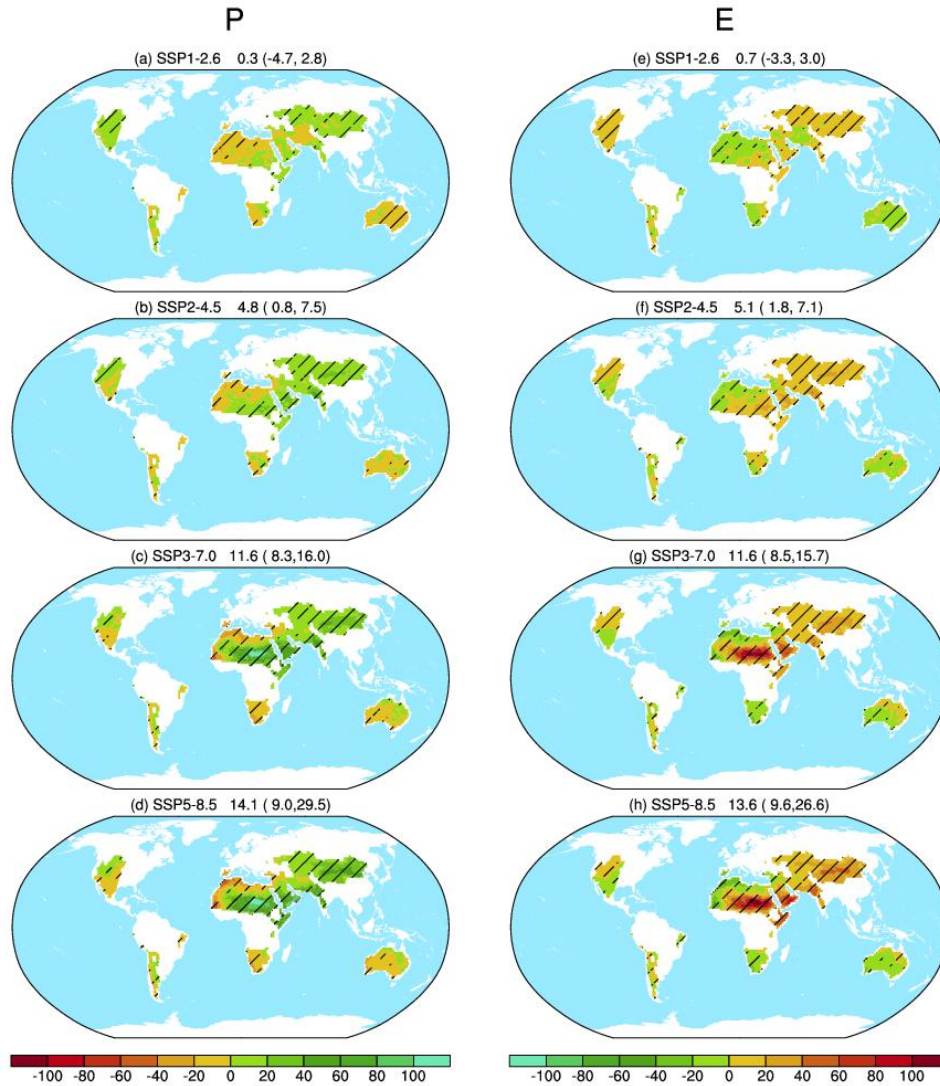
204

205 **Figure 1.** 10-year running mean of the projected changes (unit: %) in annual mean precipitation
 206 (P, a), evapotranspiration (E, b), precipitation minus evapotranspiration (P-E, c), and surface soil
 207 moisture (SM, d) across global drylands during 1960–2100, relative to 1960–1989 climatology.
 208 Historical (black), SSP1-2.6 (purple), SSP2-4.5 (blue), SSP3-7.0 (orange), and SSP5-8.5 (red)
 209 simulations are shown in median (lines) and interquartile ranges (shade).

210

211 Then we elaborate the spatial pattern of hydroclimatic changes over global drylands.
212 Figure 2 shows distributions of linear trends for annual P and E across global drylands
213 during 2015–2100 under the four different scenarios. On the whole, P and E present
214 consistent features in spatial patterns and scenario-dependent magnitudes. Under each
215 SSP scenario, P and E tend to increase over northwestern America, central and East
216 Asia, and Sahel drylands, while decrease over southwestern America, South America,
217 Mediterranean, Southern Africa, and the majority of Australia drylands. In addition,
218 the magnitudes of changes and agreements in the trend sign are intensifying with
219 warming level. Estimated from the area-averaged multimodel medians and
220 interquartile ranges, P (E) presents an overall increasing of 0.3 (-4.7, 2.8) [0.7(-3.3,
221 3.0)], 4.8 (0.8, 7.5) [5.1 (1.8, 7.1)], 11.6 (8.3, 16.0) [11.6 (8.5, 15.7)], and 14.1 (9.0,
222 29.5) [13.6 (9.6, 26.6)] %/100yr across global drylands under SSP1-2.6, SSP2-4.5,
223 SSP3-7.0, and SSP5-8.5 scenarios, respectively.

224



225

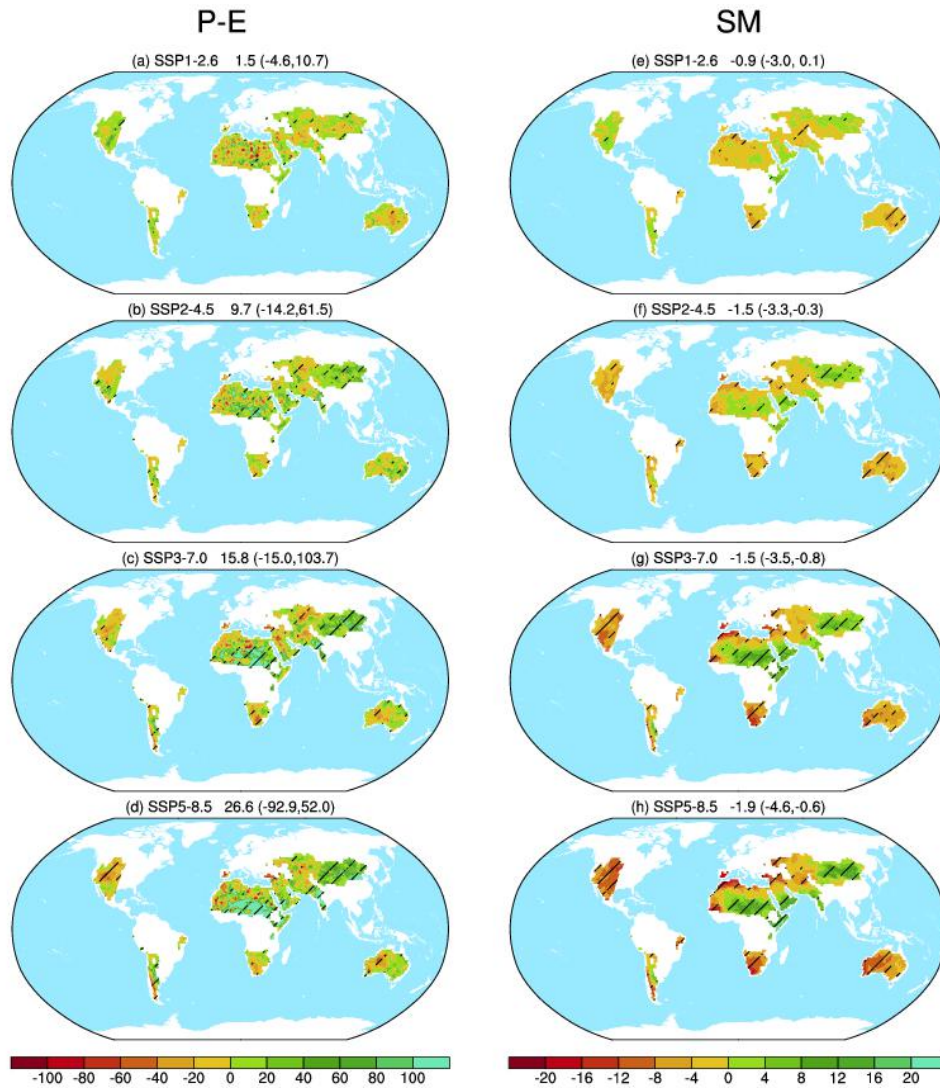
226 **Figure 2.** Multimodel medians of future linear trends (unit: %/100yr) for annual precipitation (P,
 227 a–d) and evapotranspiration (E, e–h) over global drylands during 2015–2100 under SSP1-2.6 (a,
 228 e), SSP2-4.5 (b, f), SSP3-7.0 (c, g), and SSP5-8.5 (d, h) scenarios, respectively. Slant hatchings
 229 denote where 9/13 of the CMIP6 models agree in the sign of trend. The numbers in the top of each
 230 plot are the multimodel medians and interquartile ranges of area-averaged trend across global
 231 drylands, respectively.

232

233 Figure 3 provides distributions of linear trend for annual P-E and SM over global
 234 drylands during 2015–2100 under the four different scenarios. Clearly, P-E and SM
 235 also present roughly consistent patterns and scenario-dependent magnitudes, in accord
 236 with P and E. In the 21st century, P-E and SM tend to get drying over most of the
 237 global drylands, including North America, South America, Mediterranean, central

238 Asia, Southern Africa and Australia drylands, where P decreases or increases
239 indistinctively. Conversely, obvious wetting can be seen over the regions where P
240 increases robustly, including the arid East Asia, Sahel, Middle East and South Asia.
241 Note that P-E shows more localized and divergent patterns, especially over complex
242 terrains. Area-averaged across global drylands, P-E shows a wetting of 1.5 (-4.6, 10.7),
243 9.7 (-14.2, 61.5), 15.8 (-15.0, 103.7) and 26.6 (-92.9, 52.0) %/100yr, whereas SM
244 presents a drying of -0.9 (-3.0, 0.1), -1.5 (-3.3, -0.3), -1.5 (-3.5, -0.8) and -1.9 (-4.6,
245 -0.6) %/100yr under the four different scenarios, respectively. It seems somewhat
246 paradoxical that the area-averaged P-E and SM are opposite in the future changes
247 (Figure 1c-d, Figure 3). Moreover, the inter-model uncertainties of P-E and SM are
248 also larger than P and E. These results are in line with previous studies (Dai et al.,
249 2018; Cook et al., 2020), which is mainly because water availability and SM are
250 affected by different temperature-sensitive factors (such as snow, vegetation and E)
251 and their negative feedbacks (Zhang et al., 2014; Mankin et al., 2019; Zhou et al.,
252 2021).

253



254

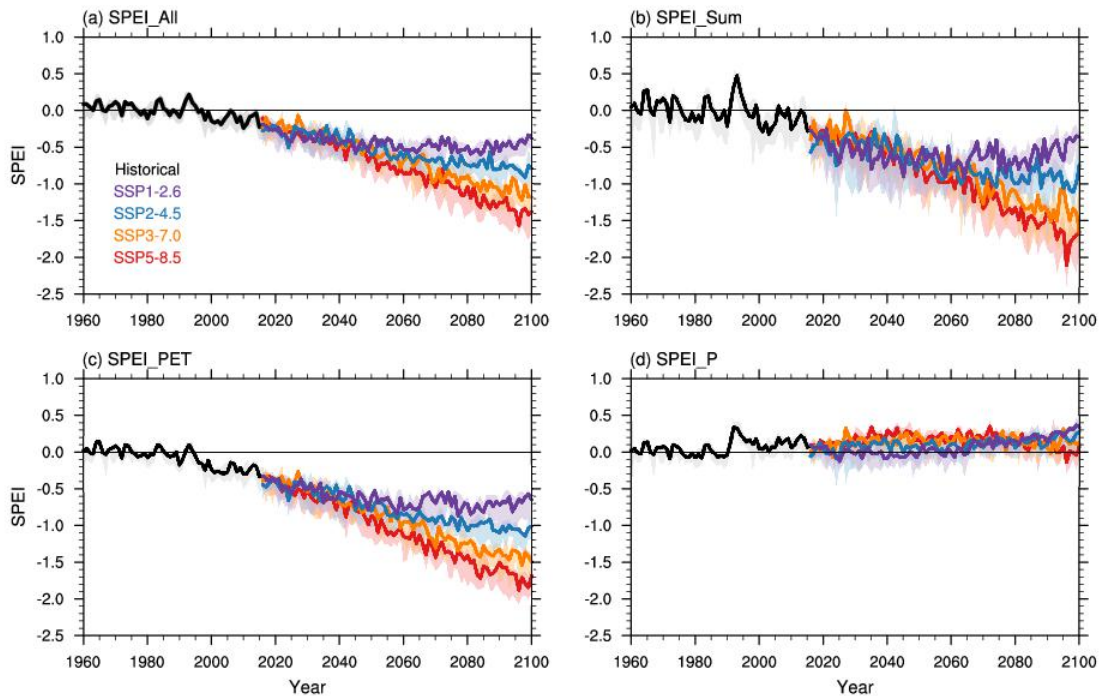
255 **Figure 3.** Same as Figure 2, but for precipitation minus evapotranspiration (P-E, a–d) and
 256 surface soil moisture (SM, e–h). Slant hatchings denote where 8/11 for SM (9/13 for P-E) of the
 257 CMIP6 models agree in the sign of trend.

258

259 3.2 Relative contributions of PET and P to drought changes

260 In this section, we use SPEI to investigate drought changes and roles of PET and P
 261 to SPEI changes in global drylands in the future projection. Before quantifying the
 262 contributions of PET and P, it is necessary to verify the reliability of SPEI for specific
 263 calculations. We first examine future changes in drought conditions via SPEI_All,
 264 SPEI_Sum, SPEI_PET and SPEI_P (Figure 4). The drought indices comprising the

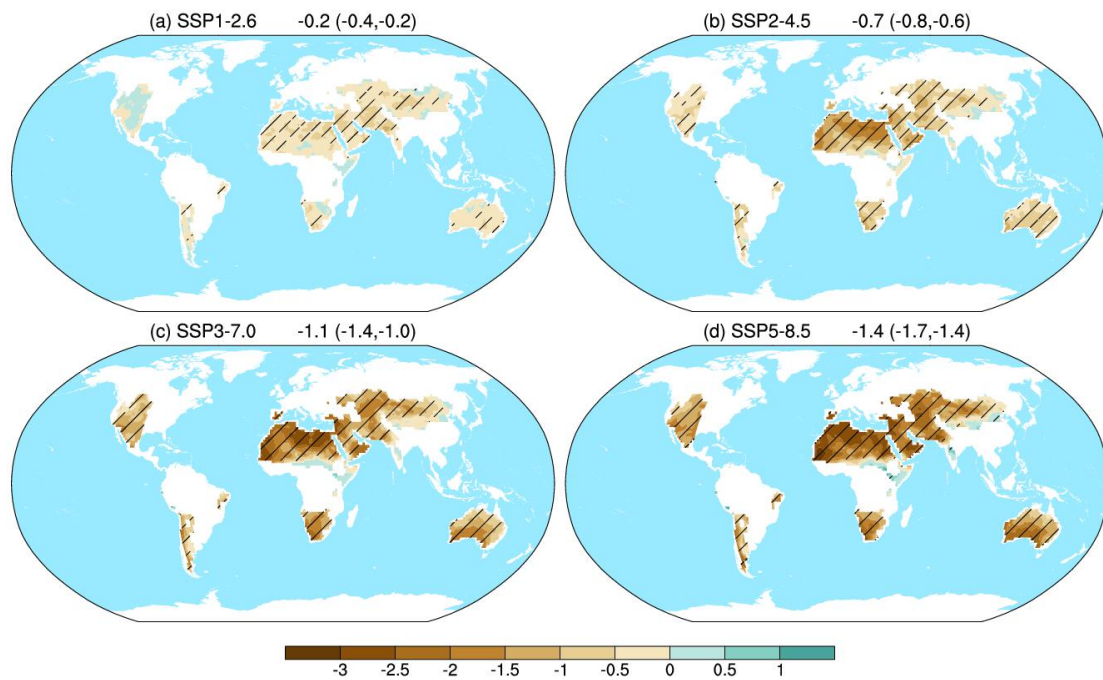
265 change of PET, i.e., SPEI_All, SPEI_Sum, SPEI_PET, tend to decline consistently in
 266 the 21st century, indicating an exacerbating drying condition because of enhanced PET.
 267 Estimated from the multimodel medians, the three indices decrease from ~0.0 in the
 268 20th century to ~ -0.5, -1.0, -1.3 and -1.5 in the end of 21st century, under SSP1-2.6,
 269 SSP2-4.5, SSP3-7.0, and SSP5-8.5 scenarios, respectively. The scenario
 270 inconsistencies are also becoming more evident with time, particularly in the second
 271 half of the 21st century. On the contrary, SPEI_P presents a very slight wetting with
 272 small scenario uncertainties.
 273



274
 275 **Figure 4.** Projected changes in annual mean (a) SPEI_All, (b) SPEI_Sum (c) SPEI_PET and (d)
 276 SPEI_P across global drylands during 1960–2100. Historical (black), SSP1-2.6 (purple), SSP2-4.5
 277 (blue), SSP3-7.0 (orange), and SSP5-8.5 (red) simulations are shown in median (lines) and
 278 interquartile ranges (shade).

279
 280 We further illustrate distributions of linear trend for annual SPEI_All (Figure 5) and
 281 SPEI for the three specific calculations (Figure 6) over global drylands during
 282 2015–2100 under the four scenarios. Unlike the above hydroclimatic fields, a
 283 widespread declining of SPEI_All can be found throughout global drylands under the

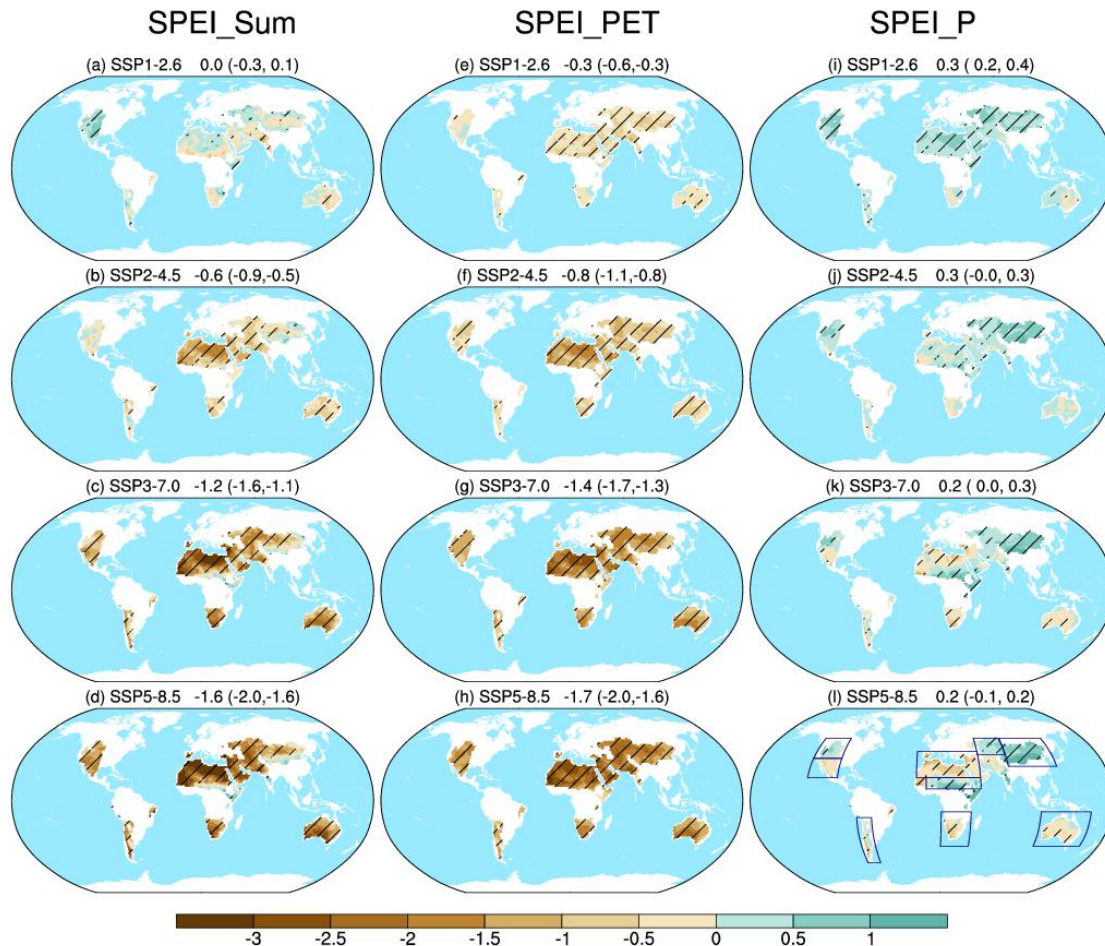
284 four scenarios (Figure 5), which is highly consistent with the substantial increasing of
 285 PET (Figures not shown). The area-averaged SPEI_All shows a drying of -0.2 (-0.4,
 286 -0.2), -0.7 (-0.8, -0.6), -1.1 (-1.4, -1.0) and -1.4 (-1.7, -1.4) /100yr under the four
 287 scenarios, respectively.
 288



289
 290 **Figure 5.** Multimodel medians of future linear trends for SPEI_All (unit: /100yr) over global
 291 drylands during 2015–2100 under SSP1-2.6 (a), SSP2-4.5 (b), SSP3-7.0 (c), and SSP5-8.5 (d)
 292 scenarios, respectively. Slant hatchings denote where 9/13 of the CMIP6 models agree in the sign
 293 of trend.

294
 295 As illustrated in Figure 6 a–d, widespread drying occurs at a rate of 0.0 (-0.3, 0.1),
 296 -0.6 (-0.9, -0.5), -1.2 (-1.6, -1.1), and -1.6 (-2.0, -1.6) /100yr throughout global
 297 drylands under the four different scenarios, respectively, estimated by the
 298 area-averaged multimodel medians and interquartile ranges. Clearly, SPEI_Sum is
 299 highly consistent with SPEI_All (Figure 5) in the spatial patterns of future drought
 300 changes, but changes a little more remarkably with relatively larger uncertainties
 301 related to scenario and model. This agrees with the validation results that the slope
 302 between SPEI_Sum and SPEI_All is slightly larger than 1.0. As for SPEI_PET

303 (Figure 6e–h), a more widespread and robust drying can be seen across the global
 304 drylands, at a rate of -0.3 (-0.6, -0.3), -0.8 (-1.1, -0.8), -1.4 (-1.7, -1.3), -1.7 (-2.0, -1.6)
 305 /100yr under the four different scenarios, respectively. SPEI_P (Figure 6 i–l) presents
 306 an overall wetting under SSP1-2.6 and SSP2-4.5 scenarios, and tends to diverse under
 307 SSP3-3.7 and SSP5-8.5 scenarios, at an area-averaged rate of 0.3 (0.2, 0.4), 0.3 (0.0,
 308 0.3), 0.2 (0.0, 0.3) and 0.2 (-0.1, 0.2) /100yr, respectively. Therefore, the derived
 309 SPEI_PET and SPEI_P can reasonably reflect the impacts of PET and P on future
 310 drought changes, respectively, and can be used to quantify the contributions of PET
 311 and P.
 312



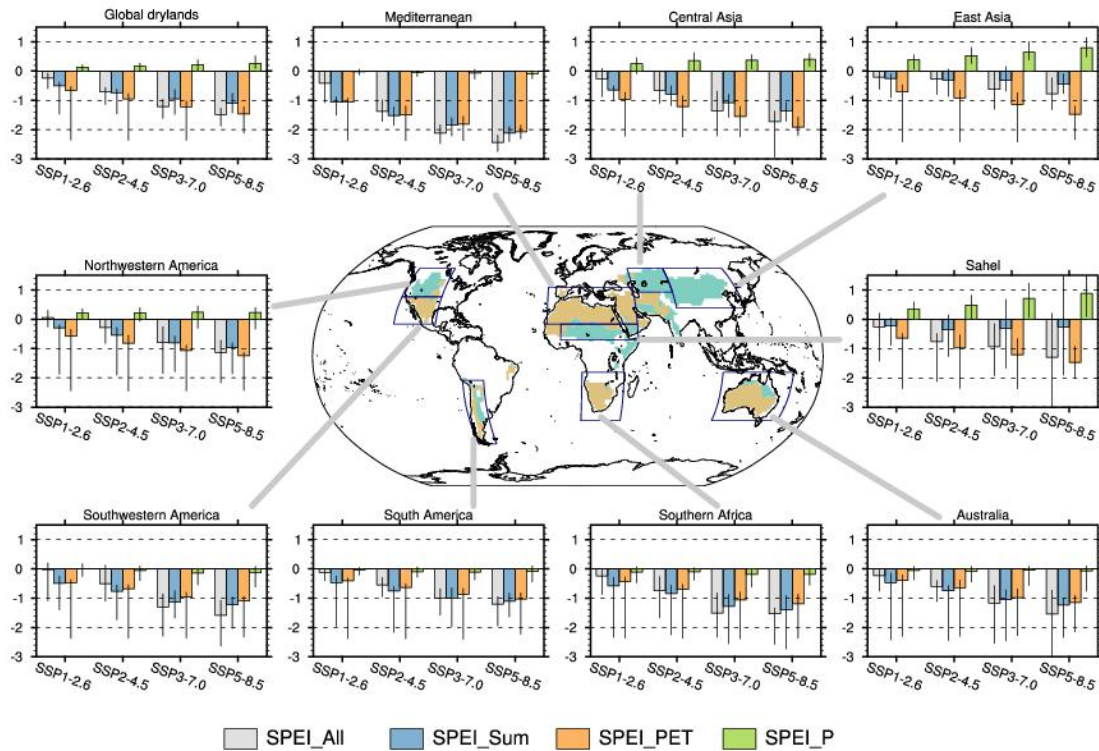
313
 314 **Figure 6.** Same as Figure 5, but for SPEI_Sum (a–d), SPEI_PET (e–h) and SPEI_P (i–l). The
 315 boxes in (l) denote the nine specific sub-drylands divided by the trend signs of SPEI_P under

316 SSP3-7.0 and SSP5-8.5 scenarios.

317

318 Under SSP3-7.0 and SSP5-8.5 scenarios, SPEI_P shows a wetting over the regions
319 where P increases significantly, including Northwestern America, central and East
320 Asia, and Sahel drylands, while drying over the regions where P decreases or
321 increases slightly, including Southwestern America and the South Hemisphere (Figure
322 6 k-l). Thus, we divide global drylands into nine sub-drylands (Figure.6 l), and
323 further investigate their area-averaged trends of the four SPEI calculations under the
324 four scenarios (Figure 7). From the perspective of global drylands, SPEI_All,
325 SPEI_Sum and SPEI_PET all see a robust drying, at a rate of -0.3, -0.5 and -0.6
326 /100yr under SSP1-2.6 scenario, -0.8, -0.8 and -1.0 /100yr under SSP2-4.5 scenario,
327 -1.2, -1.0 and -1.2 /100yr under SSP3-7.0 scenario, -1.5, -1.1 and -1.5 /100yr under
328 SSP5-8.5 scenario, respectively. However, SPEI_P experiences a slight wetting of 0.1,
329 0.15, 0.2 and 0.3 /100yr under the four scenarios, indicating the future intensifying
330 drought condition dominated by PET can be balanced by P a bit. Regionally,
331 SPEI_All, SPEI_Sum and SPEI_PET still tend to get drying but with different
332 magnitudes among sub-drylands. In particular, the drying rate in the Mediterranean is
333 nearly twice of the mean rate across global drylands. In addition, SPEI_P presents a
334 significantly regional discrepancy, declining slightly over the Mediterranean regions
335 and drylands in the South Hemisphere, while increasing over the other four
336 sub-drylands especially East Asia and Sahel drylands.

337



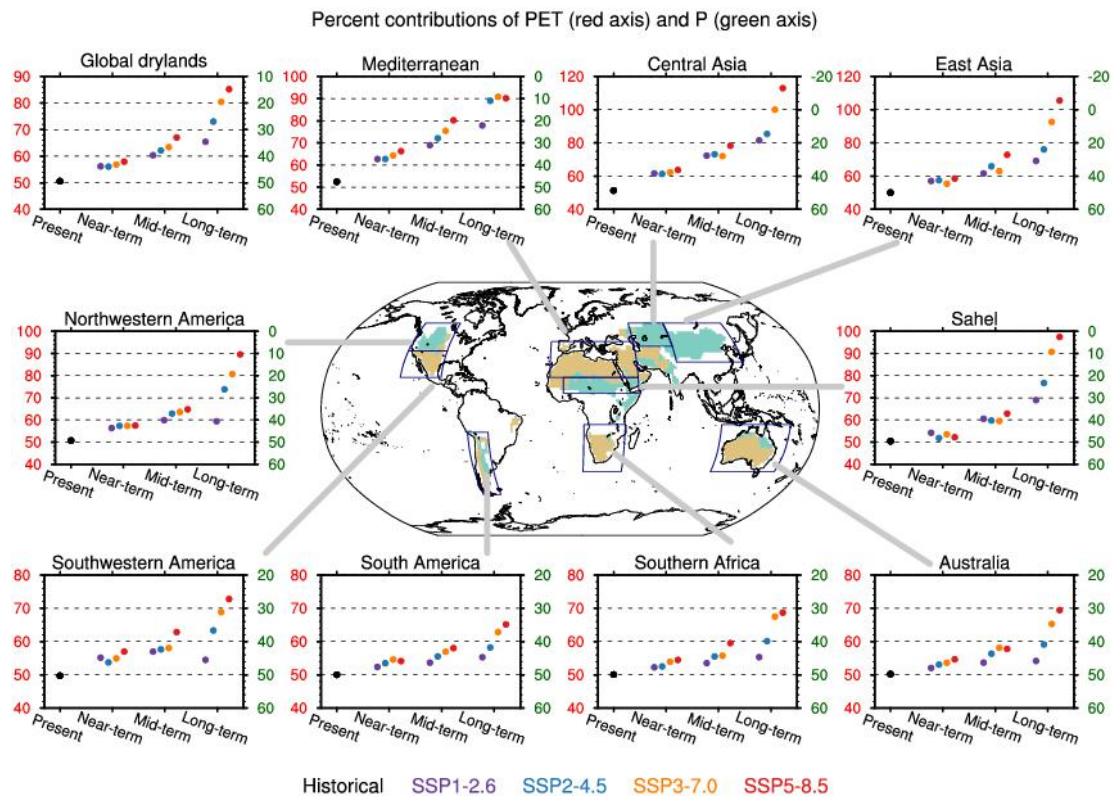
338

339 **Figure 7.** Multimodel median (bars) for trend (unit: /100yr) of SPEI_All (grey), SPEI_Sum
 340 (blue), SPEI_PET (orange) and SPEI_P (green) area-averaged over the global drylands and nine
 341 specific sub-drylands under SSP1-2.6, SSP2-4.5, SSP3-7.0, and SSP5-8.5 scenarios, respectively.
 342 The black lines indicate the interquartile ranges of the trend.

343

344 According to the formula (3–4), we obtain the contributions of PET and P to SPEI
 345 changes with respect to the 1960-1989 climatological drought condition. Figure 8
 346 illustrates the multimodel medians for fractional contributions of PET and P across the
 347 global drylands and nine sub-drylands in the four periods under different scenarios,
 348 respectively. In the present day, contributions of PET and P to SPEI changes are
 349 almost equal across the global drylands. The contribution of PET (P) increases
 350 (decreases) relatively slowly with time under SSP1-2.6 and SSP2-4.5 scenarios, while
 351 rapidly under SSP3-7.0 and SSP5-8.5 scenarios. In addition, scenario discrepancies
 352 are relatively small in the near- and mid-term, but more evident in the long-term. For
 353 near-term projections, PET (P) contributes ~58% (~42%) under the four scenarios. In
 354 the mid-term, the fractional contribution of PET (P) further increases (declines) to
 355 ~61% (~39%) under the first three scenarios, while to ~68% (~32%) under SSP5-8.5

356 scenario. In the long-term, the fractional contribution of PET (P) is relatively stable
 357 [$\sim 65\%$ ($\sim 35\%$)] under SSP1-2.6, but continue to increase (decrease) to $\sim 72\%$ (28%),
 358 $\sim 80\%$ ($\sim 20\%$), $\sim 85\%$ ($\sim 15\%$) under the other three scenarios, respectively. Regionally,
 359 the fractional contribution of PET (P) tends to increase more rapidly in the North
 360 Hemisphere than that in the South Hemisphere, especially under SSP3-7.0 and
 361 SSP5-8.5 scenarios. In particular, the contribution of PET (P) over the Mediterranean,
 362 central and East Asia drylands is much higher (lower) than the average across the
 363 global drylands. Under the two high scenarios, PET contributes to approximately or
 364 even more than 100% in the long-term due to the opposite roles of PET and P to
 365 drought changes. In the South Hemisphere, the contribution of PET (P) retains less
 366 than 70% (more than 30%) even under SSP5-8.5 because both PET and P are
 367 favorable of the intensifying drought condition.
 368



369
 370 **Figure 8.** Multimodel medians for the fractional contributions (unit: %) of PET (left axis) and P
 371 (right axis) across global drylands and nine specific sub-drylands in the present day (1995–2014),
 372 near-term (2021–2040), mid-term (2041–2060), and long-term (2081–2100), estimated from the

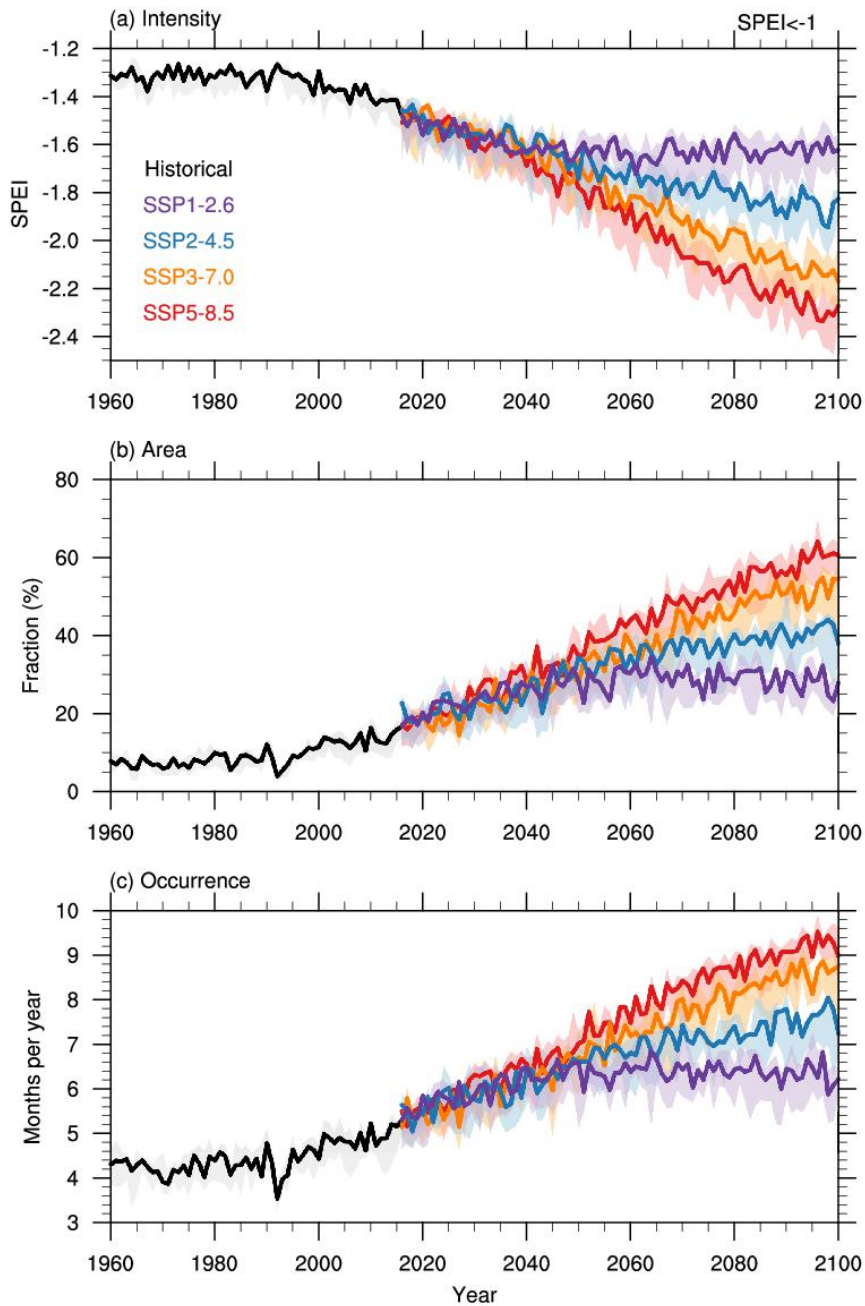
373 historical (black) simulations and SSP1-2.6 (purple), SSP2-4.5 (blue), SSP3-7.0 (orange), and
374 SSP5-8.5 (red) projections, respectively.

375

376 **3.3 Future changes in drought impacts**

377 To address detailed drought impacts and risks across global drylands for
378 policy-making, we investigate future changes in drought intensity, affected area
379 fraction and occurrence. Given severe socio-economic impacts, we focus on the
380 droughts above moderate level, i.e., SPEI_All<-1.0. Figure 9 provides the time series
381 of area-averaged drought intensity, affected area fraction and occurrence across the
382 global drylands during 1960–2100. All of the three metrics present a robust increasing
383 in the 21st century, indicating droughts will occur more intensely, widespread and
384 frequently across the global drylands. The drought intensity increases from \sim -1.3 in
385 the 20th century to \sim -1.6, -1.8, -2.1 and -2.3 in the end of 21st century, the area fraction
386 from \sim 20% to 38%, 40%, 58%, and 60%, and the occurrence from \sim 5 to 6.5, 7.5, 8.5
387 and 9.5 months per year, under SSP1-2.6, SSP2-4.5, SSP3-7.0, and SSP5-8.5
388 scenarios, respectively. The scenario inconsistencies are becoming more evident with
389 time. Notably, the drought metrics tend to be stable and alleviative in the late 21st
390 century under SSP1-2.6.

391



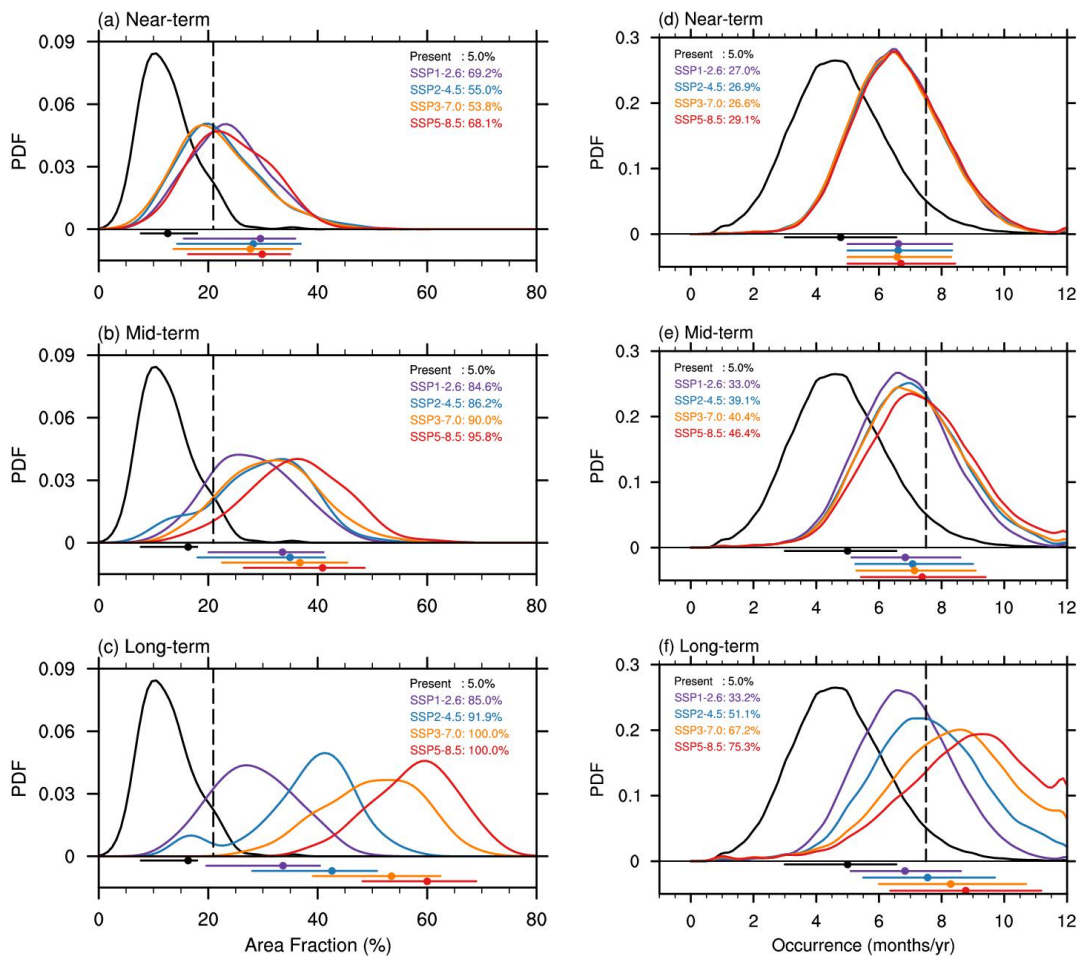
392

393 **Figure 9.** Time series of area-averaged drought (SPEI_{All<-1.0}) (a) intensity (b) affected area
 394 fraction (unit: %) and (c) occurrence (unit: months/yr) across the global drylands during
 395 1960–2100. Historical (black), SSP1-2.6 (purple), SSP2-4.5 (blue), SSP3-7.0 (orange), and
 396 SSP5-8.5 (red) simulations are shown in median (lines) and interquartile ranges (shade).

397

398 Figure 10 further provides the probability density function (PDF) changes in
 399 drought affected area fraction and occurrence in the four periods under different
 400 scenarios, respectively. Obvious shift and flattening can be seen in the future PDFs

401 compared to that in the present day. Additionally, the future PDFs tend to be divergent
 402 among scenarios with time, indicating the increasing scenario uncertainties. In
 403 particular, we use the fractional area (21%) and occurrence (7.5 months/yr) of 1-in-20
 404 years drought in the present day as thresholds to characterize extreme drought events.
 405 As to fractional area (occurrence), the probability reaches to 53.8–69.2% (27–29.1%)
 406 in the near-term, 84.6–95.8% (33–46.4%) in the mid-term, and 85.0–100%
 407 (33.2–75.3%) in the long-term under the four different scenarios, respectively. This
 408 suggests that the present-day 1-in-20-yr drought over global drylands would become
 409 dozens of times more common events, indicating that global drylands would be
 410 exposed to such severe droughts more widespread and long-lasting in the 21st century.
 411



412
 413 **Figure 10.** Probability density function (PDF) of drought affected area fraction (a–c, unit: %)

414 and occurrence (d–f, unit: months per year) across the global drylands in the near-term
415 (2021–2040, a, d), mid-term (2041–2060, b, e) and long-term (2081–2100, c, f) periods under
416 SSP1-2.6 (purple), SSP2-4.5 (blue), SSP3-7.0 (orange), and SSP5-8.5 (red) scenarios, compared
417 with the present day (1995–2014) level from the historical simulations (black). In each panel, dots
418 and horizontal lines in the bottom denote the average and the 10th to 90th range of PDFs, the black
419 dash lines present the threshold of 1-in-20-yr drought event, and the numbers indicate future
420 probabilities of such event.

421

422 **4 Conclusions and discussions**

423 In this study, we quantified the contributions of PET and P and investigated future
424 drought changes throughout the global drylands in a warming climate, using historical
425 simulations and projections under SSP1-2.6, SSP2-4.5, SSP3-7.0, SSP5-8.5 scenarios
426 from 13 CMIP6 models. The conclusions are outlined as follows.

427

428 1) The hydroclimatic fields, including P, E, P-E and SM, present consistent trend
429 distributions during 2015–2100 under the four scenarios. P-E and SM show a wetting
430 over the regions where P and E increase robustly, including the East Asia, Middle East,
431 Sahel and South Asia drylands. Likewise, P-E and SM tend to get drying over the
432 regions where P and E decreases significantly or increases indistinctively, including
433 the North America, South America, Mediterranean, central Asia, Southern Africa and
434 Australia drylands.

435

436 2) Considering changes in both P and evaporative demand (PET), the drought
437 index (SPEI) shows a widespread drying at a rate of -0.2 (-0.4, -0.2), -0.7 (-0.8, -0.6),
438 -1.1 (-1.4, -1.0) and -1.4 (-1.7, -1.4) /100yr throughout the global drylands during
439 2015–2100 under the four scenarios, respectively. By partition the impacts of PET and
440 P, we found that PET plays a critical role in drought intensification across global
441 drylands.

442

443 3) In terms of the contributions of PET and P across the global drylands, they are
444 approximately equal (~50%) to drought changes at present-day. In the 21st century, the
445 impact of PET tends to be more evident with time and warming levels. Under the four
446 scenarios, the contribution of PET (P) reaches ~58% (42%) and ~61% (~39%) in the
447 near- and mid-term, respectively, with less scenario dependence. In the long-term, the
448 contribution of PET (P) further increase to ~65% (~35%), ~72% (28%), ~80%
449 (~20%), ~85% (~15%) under SSP1-2.6, SSP2-4.5, SSP3-7.0 and SSP5-8.5,
450 respectively. In addition, the changes in contributions of PET and P show obvious
451 regional dependence due to spatial discrepancies in P changes. The contribution of
452 PET is larger in the North Hemisphere than that in the South Hemisphere. In
453 particular, it approaches to nearly 100% in the long-term under SSP5-8.5 scenario
454 over the regions where changes in PET and P offset each other, including the
455 Mediterranean, central and East Asia drylands.

456

457 4) Three drought metrics area-averaged throughout the global drylands present a
458 robust intensifying under the SSP3-7.0 and SSP5-8.5 scenarios, whereas tend to be
459 stable and somewhat alleviative under the SSP1-2.6 and SSP2-4.5 scenarios in the late
460 21st century. The drought intensity is estimated to increase from ~-1.3 at present-day
461 to ~-1.6, -1.8, -2.1 and -2.3, area fraction from ~20% to 38%, 40%, 58%, and 60%,
462 and occurrence from ~5 to ~ 6.5, 7.5, 8.5 and 9.5 months per year under the SSP1-2.6,
463 SSP2-4.5, SSP3-7.0, and SSP5-8.5 scenarios, respectively. Global drylands would be
464 exposed to severe droughts like the present-day 1-in-20-yr events more widespread
465 and long-lasting in the 21st century.

466

467 Furthermore, the following discussions should be noticed. First, we focus on the
468 present drylands measured by the climatology of AI during 1960–2018, without
469 considering the changes of dryland regions. It is undoubted that drylands would
470 expand for more intense and frequent droughts in a warming climate (Fu & Feng,
471 2013; Huang et al., 2014). Secondly, because PET and P are not entirely independent,

472 SPEI_Sum is actually higher than SPEI_All to some extent (Cook et al., 2014). Here
473 we use the first-order approximation of their relative contributions to drought changes.
474 Finally, PET is overestimated derived from model outputs (Milly & Dunne, 2016;
475 Greve et al., 2019), which maybe result in overestimating the contribution of PET to
476 drought changes. Thus, reliable constraint methods for PET correction remain to be
477 further investigated.

478

479 **Acknowledgments**

480 This study is supported by the Ministry of Science and Technology of China under
481 Grant 2018YFA0606501 and National Natural Science Foundation of China under
482 grant No. 42075037. We thank for the free open access datasets used in this study. The
483 Climatic Research Unit gridded Time Series Version 4.03 (CRU TS v.4.03) was
484 obtained from http://data.ceda.ac.uk/badc/cru/data/cru_ts/cru_ts_4.03. The CMIP6
485 simulations were obtained from <https://esgf-node.llnl.gov/search/cmip6/>. The authors
486 declare no conflict of interest.

487

488 **References**

- 489 Ault, T. R. (2020). On the essentials of drought in a changing climate. *Science*, 368, 256-260. doi:
490 10.1126/science.abc4034
- 491 Barlow, M., Zaitchik, B., Paz, S., Black, E., Evans, J., & Hoell, A. (2016). A review of drought in
492 the Middle East and Southwest Asia. *Journal of Climate*, 29, 8547-8574.
493 <https://doi.org/10.1175/JCLI-D-13-00692.1>
- 494 Berg, A., Findell, K., Lintner, B., Giannini, A., Seneviratne, S. I., van den Hurk, B., et al. (2016).
495 Land-atmosphere feedbacks amplify aridity increase over land under global warming. *Nature*
496 *Climate Change*, 6, 869–874 <https://doi.org/10.1038/nclimate3029>
- 497 Burrell, A. L., Evans, J. P., & De Kauwe, M. G. (2020). Anthropogenic climate change has driven
498 over 5 million km² of drylands towards desertification, *Nature Communications*, 11, 3853.
499 <https://doi.org/10.1038/s41467-020-17710-7>
- 500 Cook, B. I., Smerdon, J. E., Seager, R., & Coats, S. (2014). Global warming and 21st century

501 drying. *Climate Dynamics*, **43**, 2607–2627. <https://doi.org/10.1007/s00382-014-2075-y>

502 Cook, B. I., Mankin, J. S., Marvel, K., Williams, A. P., Smerdon, J. E., & Anchukaitis, K. J. (2020).
503 Twenty-first century drought projections in the CMIP6 forcing scenarios. *Earth's Future*, **8**,
504 e2019EF001461. <https://doi.org/10.1029/2019EF001461>

505 Dai, A. (2013). Increasing drought under global warming in observations and models. *Nature*
506 *Climate Change*, **3**, 52-58. <https://doi.org/10.1038/NCLIMATE1633>

507 Dai, A. (2021). Hydroclimatic trends during 1950-2018 over global land. *Climate Dynamics*,
508 <https://link.springer.com/article/10.1007/s00382-021-05684-1>.

509 Dai, A., Zhao, T., & Chen, J. (2018). Climate change and drought: A precipitation and evaporation
510 perspective. *Current Climate Change Reports*, **4**, 301 – 312. <https://doi.org/10.1007/s40641-018-0101-6>

511

512 Dai, A., & Zhao, T. (2017). Uncertainties in historical changes and future projections of drought.
513 Part I: estimates of historical drought changes. *Climatic Change*, **144**, 519-533. DOI
514 10.1007/s10584-016-1705-2

515 D’Odorico, P., & Bhattachan, A. (2012). Hydrologic variability in dryland regions: impacts on
516 ecosystem dynamics and food security. *Philosophical Transactions of the Royal Society*, **367**,
517 3145-3157. <https://doi.org/10.1098/rstb.2012.0016>

518 Eyring, V., Bony, S., Meehl, G. A., Senior, C. A., Stevens, B., Stouffer, R. J., et al. (2016).
519 Overview of the Coupled Model Intercomparison Project Phase 6 (CMIP6) experimental
520 design and organization. *Geoscientific Model Development*, **9**, 1937–1958.
521 <https://doi.org/10.5194/gmd-9-1937-2016>

522 Feng, S., & Fu, Q. (2013). Expansion of global drylands under a warming climate. *Atmospheric*
523 *Chemistry & Physics Discussions*, **13**, 14637 – 14665. doi:10.5194/acpd-13-14637-2013

524 Fragaszy, S. R., Jedd, T., Wall, N., Knutson, C., Fraj, M. B., Bergaoui, K., et al. (2020). Drought
525 monitoring in the Middle East and North Africa (MENA) region: Participatory engagement to
526 inform early warning systems, *Bulletin of the American Meteorological Society*, **101**(7),
527 E1148-E1173. <https://doi.org/10.1175/BAMS-D-18-0084.1>

528 Fu, Q., & Feng, S. (2014). Responses of terrestrial aridity to global warming, *Journal of*

529 *Geophysical Research Atmospheres*, **119**, 7863 – 7875, doi:10.1002/2014JD021608.

530 Gill, J. C., & Malamud, B. D. (2014). Reviewing and visualizing the interactions of natural
531 hazards. *Reviews of Geophysics*, *52*, 680-722, <https://doi.org/10.1002/2013RG000445>

532 Greve, P., Roderick M. L., Ukkola A. M., & Wada, Y. (2019). The aridity Index under global
533 warming. *Environmental Research Letters*, **14**, 124006.
534 <https://doi.org/10.1088/1748-9326/ab5046>

535 Hari, V., Rakovec, O., Markonis, Y., Hanel, M., & Kumar, R. (2020). Increased future occurrences
536 of the exceptional 2018-2019 Central European drought under global warming. *Scientific*
537 *Reports*, **10**,12207. <https://doi.org/10.1038/s41598-020-68872-9>

538 Harris, I., Osborn, T. J., Jones, P., & Lister, D. (2020). Version 4 of the CRU TS monthly
539 high-resolution gridded multivariate climate dataset. *Scientific Data*, **7**, 109 |
540 <https://doi.org/10.1038/s41597-020-0453-3>

541 Huang, J., Guan, X., & Ji, F. (2012). Enhanced cold-season warming in semi-arid regions.
542 *Atmospheric Chemistry and Physics*, **12**, 5391 – 5398. DOI: 10.5194/acpd-12-4627-2012

543 Huang, J., Yu, H., Guan, X., Wang, G. & Guo, R. (2015). Accelerated dryland expansion under
544 climate change. *Nature Climate Change*, **26**, 1-7. DOI: 10.1038/NCLIMATE2837

545 Huang, J., Li, Y., Fu, C., Chen, F., Fu, Q., Dai, A., et al. (2017a). Dryland climate change: Recent
546 progress and challenges. *Reviews of Geophysics*, **55**, 719–778. doi:10.1002/2016RG000550.

547 Huang, J., Yu, H., Dai, A., Wei, Y., & Kang, L. (2017b). Drylands face potential threat under 2 °C
548 global warming target. *Nature Climate Change*, **7**, 417-422. DOI: 10.1038/NCLIMATE3275

549 Huang, J., Zhang, G., Zhang, Y., Guan, X., Wei, Y., & Guo, R. (2020). Global desertification
550 vulnerability to climate change and human activities. *Land Degradation & Development*, **31**,
551 1-12. DOI: 10.1002/ldr.3556

552 Hulme, M. (1996). Recent climatic change in the world's drylands, *Geophysical Research Letters*,
553 **23**, 61–64. DOI: 10.1029/95GL03586

554 Ji, F., Wu, Z., Huang, J., & Chassignet, E. P. (2014). Evolution of land surface air temperature
555 trend. *Nature Climate Change*, **4**, DOI: 10.1038/NCLIMATE2223

556 Lehner, F., Coats, S., Stocker, T. F., Pendergrass, A. G., Sanderson, B. M., Raible, C. C., et al.
557 (2017). Projected drought risk in 1.5°C and 2°C warmer climates, *Geophysical Research*
558 *Letters*, **44**, 7419–7428, <https://doi.org/10.1002/2017GL074117>

559 Liu, Y., & Chen, J. (2021). Future global socioeconomic risk to droughts based on estimates of
560 hazard, exposure, and vulnerability in a changing climate. *Science of the Total Environment*,
561 751, 142159. <https://doi.org/10.1016/j.scitotenv.2020.142159>

562 Mannava, V.K., Sivakumar, R. L., Ramasamy, S., et al. (2013). Climate Change and Food Security
563 in West Asia and North Africa [M]. Springer.

564 Mankin, J. S., Seager, R., Smerdon, J. E., Cook, B. I., & Williams, A. P. (2019). Mid-latitude
565 freshwater availability reduced by projected vegetation responses to climate change. *Nature*
566 *Geoscience*, **12**, 983–988. <https://doi.org/10.1038/s41561-019-0480-x>

567 Miao, L., Li, S., Zhang, F., Chen, T., Shan, Y., & Zhang, Y. (2020). Future drought in the dry lands
568 of Asia under the 1.5 and 2.0 °C warming scenarios. *Earth's Future*, **8**, e2019EF001337.
569 <https://doi.org/10.1029/2019EF001337>

570 Middleton, N. J. & Thomas, D. S. G. (1992). UNEP: World atlas of desertification, Edward Arnold,
571 Sevenoaks.

572 Milly, P. C. D., & Dunne, K. A. (2016). Potential evapotranspiration and continental drying.
573 *Nature Climate Change*, **6**, 946-949. DOI: 10.1038/NCLIMATE3046

574 Monteith, J. I. L. (1965). Evaporation and Environment. *Symposia of the Society for Experimental*
575 *Biology*, **19**, 205–234.

576 O’Neill, B. C., Tebaldi, C., van Vuuren, D. P., Eyring, V., Friedlingstein, P., Hurtt, G., et al. (2016).
577 The scenario model intercomparison project (ScenarioMIP) for CMIP6. *Geoscientific Model*
578 *Development*, **9**, 3461–3482, <https://doi.org/10.5194/gmd-9-3461-2016>.

579 O’Neill, B. C., Kriegler, E., Ebi, K. L., Kemp-Benedict, E., Riahi, K., Rothman, D. S., et al.
580 (2017). The roads ahead: narratives for shared socioeconomic pathways describing world
581 futures in the 21st century. *Global Environmental Change*, **42**, 169–180.
582 <http://dx.doi.org/10.1016/j.gloenvcha.2015.01.004>

583 Penman, H. L. (1948). Natural evaporation from open water, bare soil and grass. Proceedings of

584 The Royal Society A, **193**, 120–145. DOI: 10.1098/rspa.1948.0037

585 Scheff, J., & Frierson, D. M. W. (2015). Terrestrial Aridity and Its Response to Greenhouse
586 Warming across CMIP5 Climate Models. *Journal of Climate*, **15**, 5583-5600. DOI:
587 10.1175/JCLI-D-14-00480.1

588 Schlaepfer, D., Bradford, J., Lauenroth, W., Munson, S., M., Tietjen, B., Hall, S. A., et al. (2017).
589 Climate change reduces extent of temperate drylands and intensifies drought in deep soils.
590 *Nature Communications*, **8**, 14196. <https://doi.org/10.1038/ncomms14196>

591 Sherwood, S. & Fu, Q. (2014). A drier future? *Science*, **343**, 737–739. DOI:
592 10.1126/science.1247620

593 Spinoni, J., Barbosa, P., Buchignani, E., Cassano, J., Cavazos, T., Christensen, J. H., et al. (2020).
594 Future global meteorological drought hot spots: A study based on CORDEX data. *Journal of*
595 *Climate*, **33**, 3635-3661. DOI: 10.1175/JCLI-D-19-0084.1

596 Takeshima, A., Kim, H., Shiogama, H., Lierhammer, L., Scinocca, J. F., Seland, Ø., et al. (2020).
597 Global aridity changes due to differences in surface energy and water balance between 1.5 °C
598 and 2 °C warming. *Environmental Research Letters*, **15**, 0940a7.
599 <https://doi.org/10.1088/1748-9326/ab9db3>

600 Trenberth, K. E, Dai, A., van der Schrier, G., Jones, P. D., Barichivich, J., Briffa, K. R., et al.
601 (2014). Global warming and changes in drought. *Nature Climate Change*, **4**, 17-22.
602 <https://doi.org/10.1038/NCLIMATE2067>

603 Ukkola, A. M., De Kauwe, M. G., Roderick, M. L., Abramowitz, G., & Pitman, A. J. (2020).
604 Robust future changes in meteorological drought in CMIP6 projections despite uncertainty in
605 precipitation. *Geophysical Research Letters*, **46**, e2020GL087820. [https://doi.](https://doi.org/10.1029/2020GL087820)
606 [org/10.1029/2020GL087820](https://doi.org/10.1029/2020GL087820)

607 United Nations Development Programme (UNDP). (2014), Environment and energy, drylands
608 development centre, where we work, Accessed 19 Jan 2014.

609 Vicente-Serrano, S. M., Beguería, S. & López-Moreno, J. I. (2010). A multiscalar drought index
610 sensitive to global warming: the standardized precipitation evapotranspiration index. *Journal*
611 *of Climate*, **23**, 1696 - 1718. DOI:10.1175/2009JCLI2909.1

612 Vicente-Serrano, S. M., Beguería, S. & López-Moreno, J. I. (2012). Performance of Drought
613 Indices for Ecological, Agricultural, and Hydrological Applications. *Earth Interactions*, **16**,
614 1-27. DOI: 10.1175/2012EI000434.1

615 Vicente-Serrano, S. M., Quiring S. M., Peña-Gallardo M., Yuan S., & Domínguez-Castro F. (2020).
616 A review of environmental droughts: Increased risk under global warming? *Earth-Science*
617 *Reviews*, 201, 102953. <https://doi.org/10.1016/j.earscirev.2019.102953>

618 Wei, Y., Yu, H., Huang, J., Zhou, T., Zhang, M., & Ren, Y. (2019). Drylands climate response to
619 transient and stabilized 2 °C and 1.5 °C global warming targets. *Climate Dynamics*, **53**,
620 2375–2389. <https://doi.org/10.1007/s00382-019-04860-8>

621 White, R. P., & Nackoney, J. (2003). *Drylands, People and Ecosystem Goods and Services*, World
622 Resources Institute, Washington.

623 Xie, R. H., & Wang, A. H. (2020). Comparison of ten potential evapotranspiration models and
624 their attribution analyses for ten Chinese drainage basins. *Advances in Atmospheric Sciences*,
625 **37**, 959–974. <https://doi.org/10.1007/s00376-020-2105-0>.

626 Yao, J., Liu, H., Huang, J., Gao, Z., Wang, G., Li, D., et al. (2020). Accelerated dryland expansion
627 regulates future variability in dryland gross primary production. *Nature Communications*, **11**,
628 1665. <https://doi.org/10.1038/s41467-020-15515-2>

629 Zhang, X., Tang, Q., Zhang, X., & Lettenmaier, D. P. (2014). Runoff sensitivity to global mean
630 temperature change in the CMIP5 Models. *Geophysical Research Letters*, **41**, 5492–5498.
631 <https://doi.org/10.1002/2014GL060382>

632 Zhao, T., & Dai, A. (2017). Uncertainties in historical changes and future projections of drought.
633 Part II: model-simulated historical and future drought changes. *Climatic Change*, **144**,
634 535-548. DOI 10.1007/s10584-016-1742-x

635 Zhou, S., Zhang, Y., Williams, A. P., & Gentile, P. (2019). Projected increases in intensity,
636 frequency, and terrestrial carbon costs of compound drought and aridity events. *Science*
637 *Advances*, **5**, eaau5740. DOI: 10.1126/sciadv.aau5740

638 Zhou, S., Williams, A.P., Lintner, B.R., Berg, A. M., Zhang, Y., Keenan T. F., et al. (2021). Soil
639 moisture–atmosphere feedbacks mitigate declining water availability in drylands. *Nature*
640 *Climate Change*, **11**, 38–44. <https://doi.org/10.1038/s41558-020-00945-z>

641 Zotarelli, L., Dukes, M. D., Migliaccio, K. W., & Morgan, A. K. T. (2013). Step by Step
642 Calculation of the Penman-Monteith Evapotranspiration (FAO-56 Method) www:
643 <http://edis.ifas.ufl.edu/pdffiles/ae/ae45900.pdf>